euronoise

Acoustic characterization of an ultrasound surgical transmitter in the linear and nonlinear regime of working

Antonio Petosic[a], Bojan Ivančević[a] and Dragoljub Svilar[b]

[a]Faculty of Electrical Engineering and Computing, Unska 3, 10000 Zagreb, Croatia
[b]Brodarski Institut, Avenija Većeslava Holjevca bb, 10000 Zagreb, Croatia
antonio.petosic@fer.hr

The method for measurement of a derived acoustic power of an ultrasound surgical knife has been suggested in the free acoustic field conditions. The pressure field of the transmitter, immersed in depth of quater wavelength and vibrating at the fundamental frequency (≈25 kHz), has been measured with calibrated hydrophone system at different electrical excitation levels. In the linear regime, the transmitter has been theoretically described as an acoustic dipole. The radiated acoustic power, displacement and velocity magnitude at excitation frequency has been found, and good agreement between theoretical and experimental results is obtained. When transmitter is excited with higher electrical power levels, the nonlinear behaviour in loading medium appears, with strong cavitation activity. In the averaged power spectrum of the recorded acoustic pressure signal is evident the presence of harmonics ($n \cdot f$), subharmonics (f/q), ultraharmonics ($n \cdot f/q$) of excitation frequency, and also the presence of cavitation noise with continouus frequency components even up to twentieth harmonic of fundamental frequency. The spatial pressure distribution of each discrete frequency component in the free acoustic field has been measured and its contribution to total acoustic power has been calculated.

1 Introduction

In this work measurement of derived acoustic power has been considered using calibrated hydrophone measurement system. The transmitter with sonotrode tip has been immersed at quarter wavelength (d= λ/4) on the working frequency (f_0=24670 Hz) in the anechoic pool at Brodarski Institute (Fig 1.). The spatial distribution of pressure magnitude has been measured at different frequency components in z and y direction. In the linear regime of working only excitation frequency component appears in the pressure waveform signal [1]. In the nonlinear regime in front of sonotrode tip, dominant nonlinear effect is cavitation. Subharmonics, harmonics and ultraharmonics appear in the recorded waveform signal in front of the sonotrode tip.

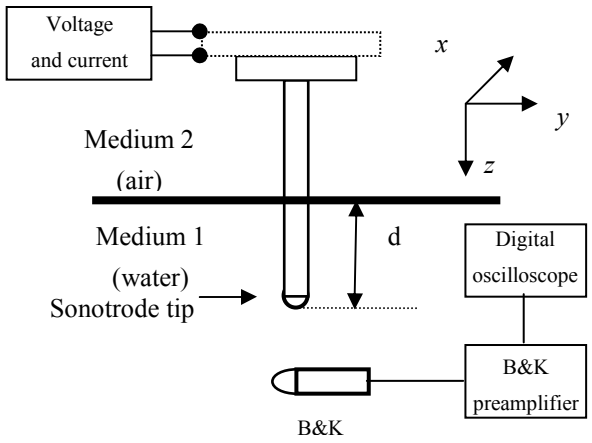

Fig. 1. Ultrasound point source in the free acoustic field

The signal processing techniques have been used to obtain pressure magnitudes in the acoustic field points at each frequency component of interest. In the linear regime of working only excitation frequency is present in the signal of dynamical acoustic pressure.

At higher excitation levels, nonlinear effects in loading medium appear: acoustic streaming, finite amplitude effects and cavitation [2-4].The dominant effect is cavitation due to nonlinear oscillations of air bubbles in the fluid. The discrete frequency components (subharmonics, harmonics and ultraharmonics) appear in the power spectrum of dynamic acoustic pressure [5].

In the linear regime of working the non-ideal source (sonotrode tip) has been modelled as radially and transversally oscillating sphere [6]. The parameters of ideal source (source velocity and displacement magnitude) are found using acoustic reciprocity theory, assuming point source near pressure relase boundary (water-air boundary) [7]. In the nonlinear regime the discrete and continouus frequency components appear and it has been seen that average magnitude of pressure at each discrete frequency component of interest has spatial distribution in the form of C/r.

2 Linear modeling

In this part of work the models of radially and transversally oscillating spheres have been analyzed in linear acoustic approximation [8].

2.1 Radially oscillating sphere

Assuming that sonotrode tip is a point source of ultrasound with dimensions much smaller than wavelength (λ= 6cm) in the medium at fundamental excitation frequency (f_0= 24670 Hz).

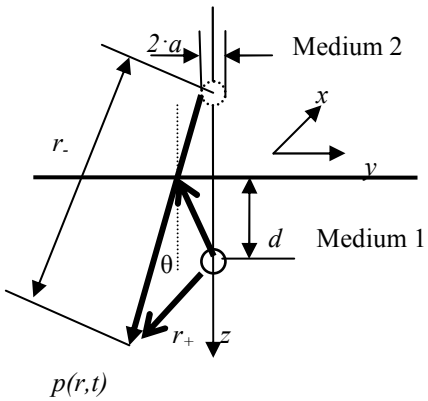

Fig. 2. Radially oscillating sphere near pressure release boundary

The direct pressure field from real source (with radius a) can be written in the form of eq. 1.

$$\hat{p}_d(r_+,t)=\frac{\hat{Q}_0\cdot k\cdot\rho_0\cdot c_0}{4\cdot\pi\cdot(k\cdot a-j)\cdot r_+}\cdot e^{j\cdot[\omega\cdot t-(k\cdot r_+-k\cdot a)]} \quad (1)$$

$$\hat{p}_d(r_+,t)=\frac{\hat{A}_d}{r_+}\cdot e^{-j\cdot[(k\cdot r_+-k\cdot a)]}\cdot e^{j\cdot\omega\cdot t}\quad r_+\geq a$$

r_+ [m]- distance from real sourc to field point

d [m]- immersion depth

$\hat{Q}_0$ [m^3/s]- volume source strength

ρ_0 [m^3/s]- densitiy of loading medium (water)

c_0 [m/s]- ultrasound velocity in water

k [m^{-1}]- wavenumber in water

a [m]- radius of theoretical radially oscillating sphere

Pressure from image of the source p_r is given in the form of eq. 2.

$$\hat{p}_r(r_-,t)=\frac{\hat{A}_r}{r_-}\cdot e^{-j\cdot[k\cdot r_--k\cdot a]} \quad (2)$$

The total pressure in the acoustic field point is given in the form of eq. 3.

$$\hat{p}(r)=\hat{p}_d(r_+)+\hat{p}_r(r_-)=\frac{\hat{A}}{r_+}\cdot e^{-j\cdot[(k\cdot r_+-k\cdot a)]}+R(\theta)\cdot\frac{\hat{A}}{r_-}\cdot e^{-j\cdot[k\cdot r_--k\cdot a]} \quad (3)$$

R(θ)- coefficient of reflection given in the form of eq. 4.

$$R(\theta)=\frac{Z_2\cdot\cos(\theta_i)-Z_1\cdot\cos(\theta_t)}{Z_2\cdot\cos(\theta_i)+Z_1\cdot\cos(\theta_t)} \quad (4)$$

Z_2 [kg/m^{2}s]- characteristic acoustic impedance of medium 2

Z_1 [kg/m^{2}s]- characteristic acoustic impedance of medium 1

The pressure magnitude is measured in the free field in *z*-direction and connection velocity potential functions of two sources have been used to find pressure field on axis *z*.

The velocity potential $\psi(t)$ is given in the form of equation 4, when volume strength source magnitude (Q_0) is unknown.

$$\psi(z)=-\frac{Q_0}{4\cdot\pi\cdot(z-d)}\cdot e^{-j\cdot k\cdot(z-d)}+\frac{Q_0}{4\cdot\pi\cdot(z+d)}\cdot e^{-j\cdot k\cdot(z+d)} \quad (4)$$

Using connection between pressure and velocity potential in form of eq. 5 the pressure is found.

$$p=-\rho_0\cdot\frac{d\psi}{dt}\Rightarrow\hat{p}-j\cdot\omega\cdot\rho_0\cdot\hat{\psi} \quad (5)$$

The pressure assuming far field approximation and only difference in phase between real source and its image is given with eq. 6.

$$P(z)=\frac{\rho_0\cdot f\cdot Q_0}{z}\cdot\sin(k\cdot d)=\frac{\rho_0\cdot c_0\cdot k\cdot Q_0}{2\cdot\pi\cdot z}=\frac{C}{z} \quad (6)$$

f [Hz]- working frequency

$P(z)$ [Pa]- pressure magnitude

C [Pa] - approximation parameter

When immersion depth $d=\lambda/4$ than value $\sin(k\cdot d)=1$.

Approximating the pressure magnitude spatial dependency $P(z)$ using eq. 6, the volume strength of the source and other parameters of the equivalent source can be easily found at different transmitter excitation levels. The results of fitting are shown on fig. 3.

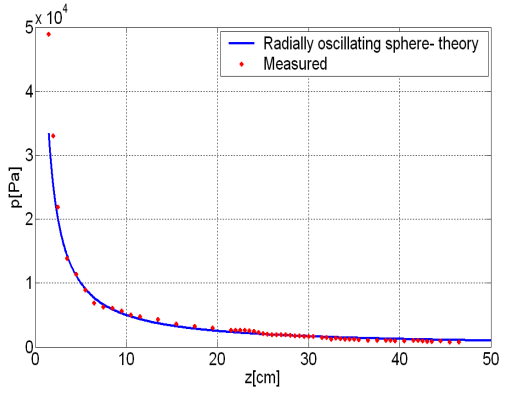

Fig. 3. Fitting measured pressure magnitude spatial distribution with theoretical curve

Applied RMS electrical power in considered case is P_{EL}=0.62 W. The approximation parameter measured in this case C= 500.2 Pa·m. Volume strength magnitude calculated from C is Q_0=2.033·10^{-5} m^3/s. The derived acoustic power (P_d) is calculated using eq. 7 and it has value P_d= 0.263 W. The electroacoustic efficiency factor (η_{ea}) is calculated as ratio of derived and applied acoustic power and it is η_{ea}= 40 %.

$$P_d=\frac{\rho_0\cdot c_0\cdot k^2}{8\cdot\pi}\cdot {Q_0}^2 \quad (7)$$

Knowing source volume strength magnitude, the velocity and displacement magnitudes of radially oscillatng sphere can be calculated using equations 8 and 9.

$$\vec{\hat{u}}(r=a,t)=\hat{U}_0\cdot e^{j\cdot\omega\cdot t}\cdot\vec{r}$$
$$\hat{U}_0=\frac{\hat{Q}_0\cdot k}{4\cdot\pi\cdot a\cdot(k\cdot a-j)}\cdot\left(1-\frac{j}{k\cdot a}\right) \quad (8)$$

In the linear regime of working the connection between velocity anf displacement is given using eq. 9.

$$u(t)=\frac{d\xi}{dt}\Rightarrow\hat{U}_0=j\cdot\omega\cdot\hat{\xi}_0\Rightarrow\hat{\xi}_0=\frac{\hat{U}_0}{j\cdot\omega} \quad (9)$$

Magnitude of velocity on the radially oscillating surface U_0= 0.67 m/s and displacement magnitude on the source is ξ_0= 1.67 µm.

The pressure field calculated assuming radially oscillating sphere near pressure release boundary is shown on fig. 4.

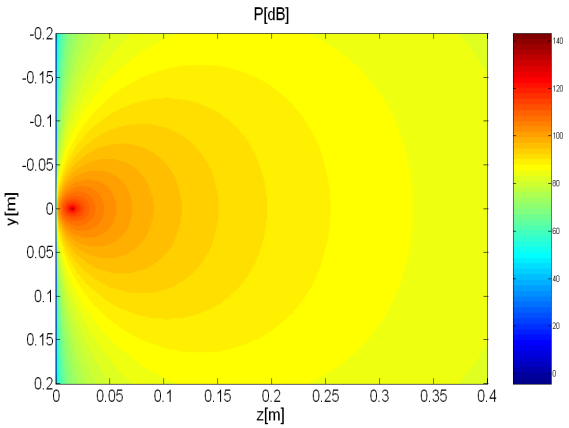

Fig. 4. Pressure field magnitude of radially oscillating sphere near pressure release boundary

The velocity potential function on *z*-axis is shown on fig. 5.

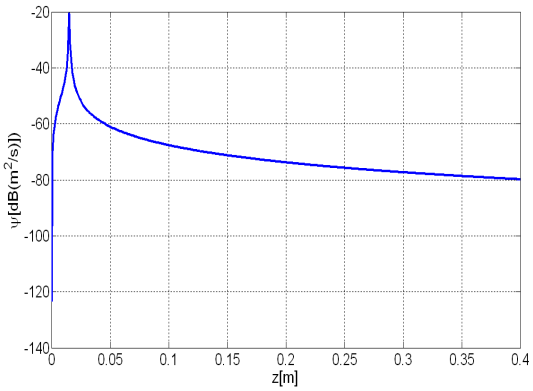

Fig. 5. Velocity potential of radially oscillating sphere near pressure release boundary

It can be seen on fig. 5 that gradient of velocity potential ($\vec{u} = \nabla\psi$) near pressure release boundary is high. That means that velocity (u) is dominant to the pressure ($p \approx 0$).

2.2 Transversally oscillating sphere

The next theoretical model considered is transversally oscillating sphere. The pressure magnitude spatial distribution approximation parameter C is same as in radially oscillating sphere model, but velocity and displacement magnitude of sources aren't same due to different equations describing model.

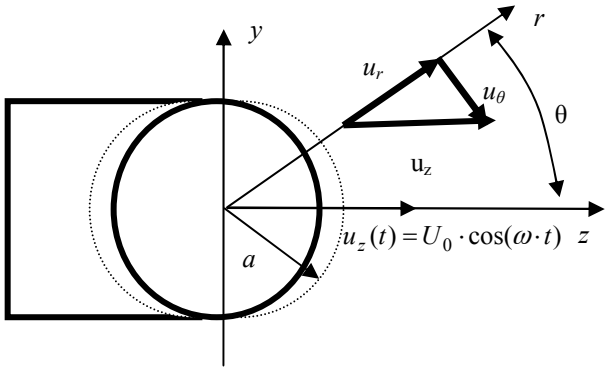

Fig 6. The tip of sonotrode as transversally oscillating sphere

The pressure field of isolated transversally oscillating sphere can be written in the form of eq. 8.

$$\hat{p}(r,\theta) = \rho_0 \cdot \omega \cdot \hat{A} \cdot \cos\theta \cdot \frac{j \cdot e^{-j \cdot k \cdot r}}{r} \cdot \left[\frac{1}{r} + j \cdot k\right] \quad (8)$$

It can be ssen that pressure field depends on angle θ and source parameter A. The parameter A is given in the form of eq. 9.

$$\hat{A} = \frac{\hat{U}_0 \cdot a^3 \cdot e^{j \cdot k \cdot a}}{2 - (k \cdot a)^2 + 2 \cdot j \cdot k \cdot a} \quad (9)$$

The total pressure field assuming superposition of direct and reflected waves (from pressure release boundary) is given with eq. 10.

$$p(r,\theta) = \frac{\omega^2 \cdot \rho_0}{c_0} \cdot \cos(\theta) \cdot A \cdot \frac{e^{-j \cdot (k \cdot r_+ - k \cdot a)}}{r_+} + R(\theta) \cdot \frac{\omega^2 \cdot \rho_0}{c_0} \cdot \cos(\theta) \cdot A \cdot \frac{e^{-j \cdot (k \cdot r_- - k \cdot a)}}{r_-}$$

In the far field approximation the expression isn't so complicated and it is given with expression 11.

$$p(r,\theta) = 2 \cdot j \cdot \frac{\omega^2 \cdot \rho_0}{c_0} \cdot \cos(\theta) \cdot A \cdot \frac{e^{-j \cdot (k \cdot r)}}{r} \sin[k \cdot d \cdot \cos(\theta)] \quad (11)$$

In the z- direction $\theta = 0°$ and the expression for pressure magnitude can be fitted with C/z function.
Velocity magnitude $U_0 = 2$ m/s and displacement magnitude $\xi_0 = 13$ μm. These values are higher than in the case of radially oscillating sphere as consequence of vibrating body only in z- direction.
The theoretical pressure magnitude spatial distribution in y direction of radially and transversally oscillating sphere is compared with experimental on fig 7.

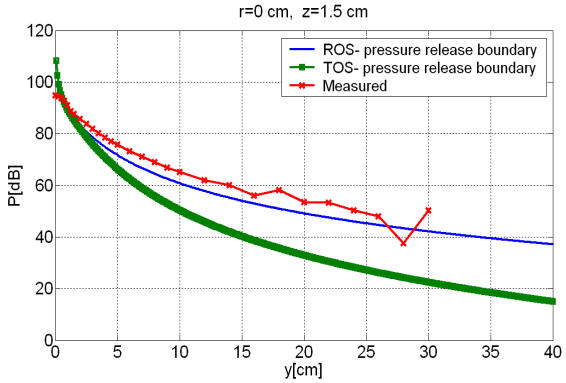

Fig. 7. Presure magnitude spatial distribution on axis y at r=0 cm

The results of comparison at distance r=10 cm from sonotrode tip are shown on fig. 8.

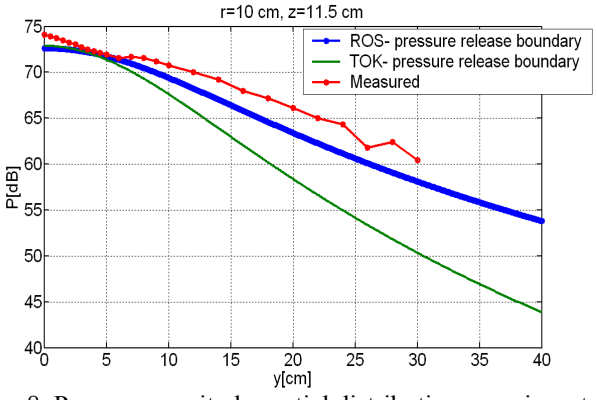

Fig. 8. Presure magnitude spatial distribution on axis y at z=11.5 cm

From results on figures 7 and 8 it can be seen that better model is radially oscillating sphere due to geometry of sonotrode tip (half of the sphere)..
The results for equivalent theoretical models in the form of radially oscillating sphere for different excitation levels are shown in table 1.

P_{EL}[W]	U_0[m/s]	ξ_0[μm]	P_d[W]	η_{ea}[%]
0.65	0.26	1.67	0.26	40.0
1.37	0.39	2.51	0.59	43.5

Table 1. Parameters of radially oscillating sphere calculated for the US source working in the linear regime

It can be seen from table 1. that electroacoustic efficiency factor is 40%. It will be very interesting to see how this factor can be calculated in the nonlinear regime of transmitter working when stable and transient cavitation are present in the operating medium.

3 Nonlinear regime of working

The linear model has been suggested in the nonlinear regime of working assuming that all nonlinear sources (oscillating bubbles) are in the vicinity of sonotrode tip. The parameters of medium are unchanged in the far field. The pressure waveforms have been recorded in the fields on *z*-axis at different electrical excitation levels. The pressure waveform is recorded at *r*= 1cm at two different levels of excitation are shown on fig. 9.

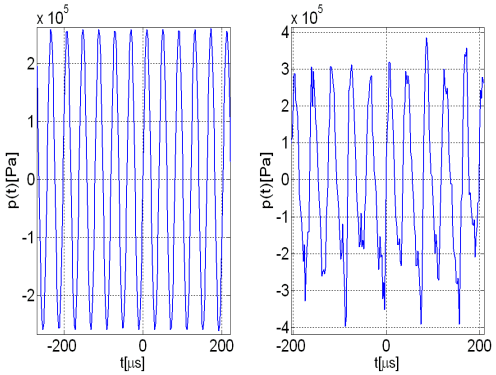

Figure 9. Pressure waveforms recorded in the acoustic field at two different levels of excitation (left-linear, right-nonlinear)

The modern processing technique (*welch* method) is used to calculate power signal density. The results for two different levels of excitation are shown on fig. 10.

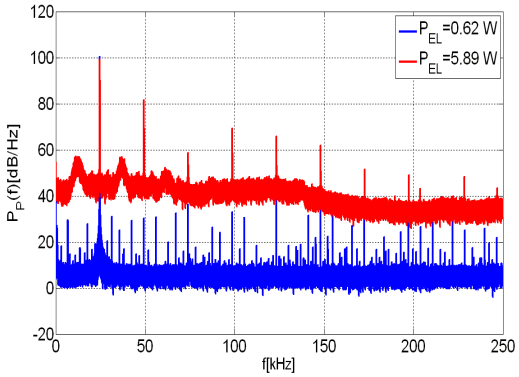

Fig. 10. Power spectrum densities of recorded pressure waveforms at different excitation levels

It is evident difference between pressure magnitudes of frequency components in the signal. The power spectrum magnitude is transformed to pressure magnitude at each frequency component. The same calculation, as suggested in linear model, is applied for each discrete frequency component of interest.
The total pressure magnitude is suggested as sum of each individual frequency component in the form of eq. 12.

$$p(r,t) \equiv P_1 \cdot e^{j(\omega_1 t+\varphi_1)} \cdot e^{-j \cdot k_1 \cdot r} + P_2 \cdot e^{j(\omega_2 t+\varphi_2)} \cdot e^{-j \cdot k_2 \cdot r} + P_3 \cdot e^{j(\omega_3 t+\varphi_3)} \cdot e^{-j \cdot k_3 \cdot r} + \ldots.$$

$$p(r,t) \equiv \sum_{i=1}^{n} P_i \cdot e^{j(\omega_i t+\varphi_n)} \cdot e^{-j \cdot k_i \cdot r}$$

(12)

n- number of frequency components in discrete spectrum representation

Knowing pressure magnitude at each frequency component of interest ($P(\omega_i)$) and assuming that parameters of medium aren't changed in the far field due to cavitation, the volume strength of the sources on each discrete frequency component of interest is given in the form of equation 13.

$$\left|Q_i(\omega_i)\right| = \left| \frac{4 \cdot \pi \cdot z \cdot \left|P(\omega_i)\right|}{j \cdot \rho_0 \cdot \omega_i \cdot \left(\frac{e^{-j \cdot k \cdot d}}{z-d} + \frac{e^{+j \cdot k \cdot d}}{z+d} \right)} \right| \qquad (13)$$

The derived acoustic power on each can be calculated knowing volume strength of source in the form of eq. 14.

$$P_{id}(\omega_i) = \left(\frac{\rho_0 \cdot c_0 \cdot k_i^2(\omega_i)}{8 \cdot \pi} \right) \cdot \left| Q_i^2(\omega_i) \right|^2 \qquad (14)$$

The applied procedure for calculating derived acoustic power on each frequency component is shown on fig. 11.

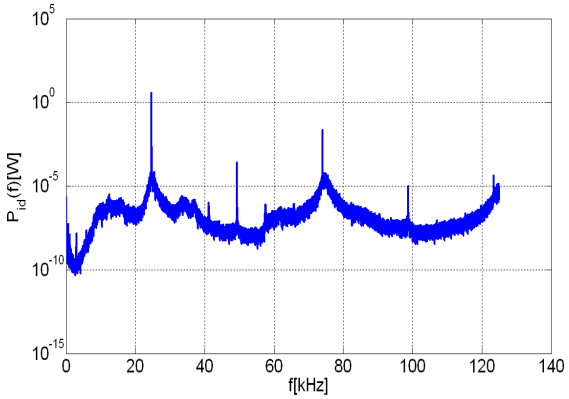

Fig. 11. Derived acoustic power on each frequency component of interest in the nonlinear regime

The radiated acoustic power on excitation frequency is dominant and it is several magnitudes higher than power on other frequency components. The results for calculated derived acoustic power on some discrete frequency components are shown in the table 2.

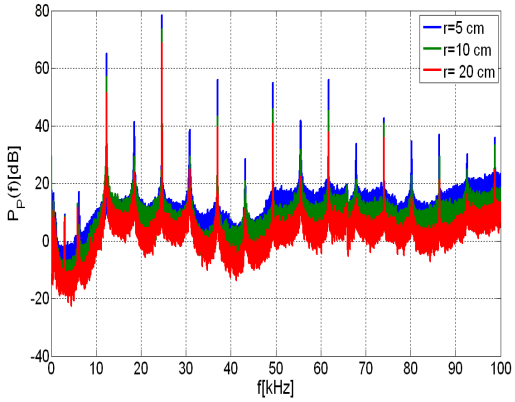

Fig. 12. Pressure magnitude spatial distribution at each frequency component of interest

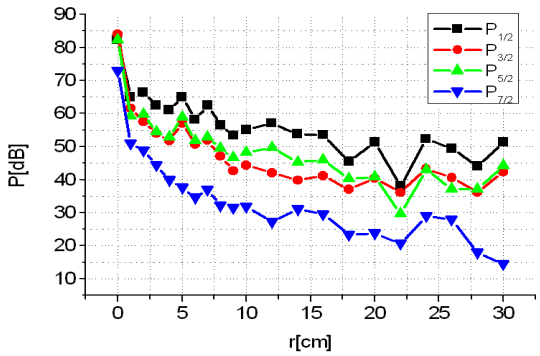

Figure 13. Pressure magnitude distribution of subharmonics

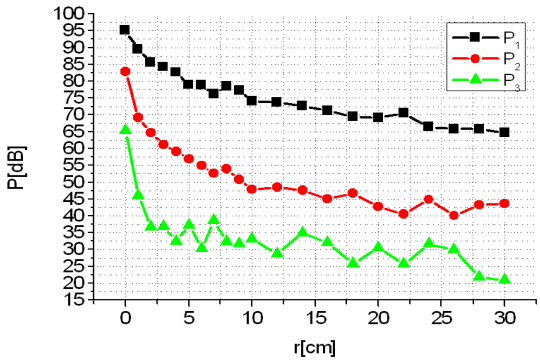

Figure 14. Pressure magnitude spatial distribution for harmonics

The fitting pressure magnitude spatial distribution with theoretical curve in the form of C/z for considered applied electrical power is shown on figure 15.

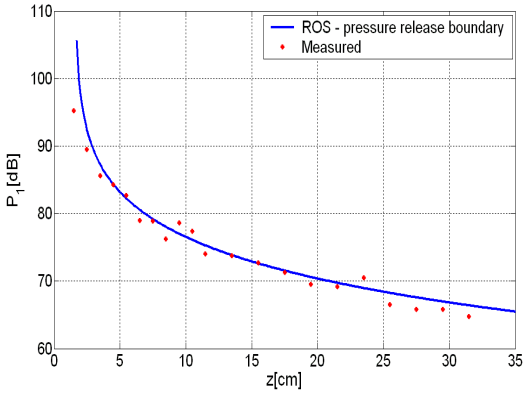

Fig. 15. Pressure magnitude spatial distribution and comparison with theoretical results (f_0)

It can be seen that spatial distribution of magnitudes can be very well fitted with theoretical law, and parameters of equivalent radially oscillating sources on each discrete frequency components can be found.
The results of theoretical fitting for fundamental frequency are shown in table 2.

P_{EL}[W]	U_0[m/s]	ξ_0[μm]	P_d[W]	η_{ea}[%]
1.89	0.34	2.18	0.451	23.86

Table 2. Fitting parameters of theoretical source on f_0

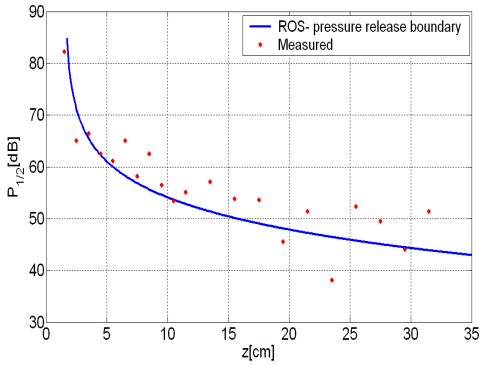

Fig. 16. Pressure magnitude spatial distribution and comparison with theoretical results ($f_{1/2}$)

In the table 3 the fitting results are shown for $f_{1/2}$.

P_{EL}[W]	$U_{01/2}$[m/s]	$\xi_{01/2}$[μm]	$P_{d1/2}$[mW]
1.89	0.073	0.94	5.2

Table 3. Fitting parameters on subharmonic frequency

The majority of acoustic power is on fundamental frequency (f_0)..

4 Conclusion

It can be seen that in nonlinear egime of working the electroacoustic efficiency factor is decreased from 40 % to 23 % and in next steps the more applied electrical power levels will be considered. In future work the same procedure will be repeated for different types of sonotrode tips and more applied electrical powers values

References

[1] Acoustical characterization of ultrasonic surgical device.IEEE Ultrasonic symposium, 1995.
[2] Beyer RT. Nonlinear Acoustics. American Journal of Physics 1973; 41(9):1060-1067.
[3] Hamilton M.F., Blackstock D.T.: On the Coefficient of Nonlinearity-B in Nonlinear Acoustics,JASA 1988; 83(1):74-77.
[4] Hamilton M.F., Blackstock D.T.: Nonlinear acoustics. American Institute of Physics, 1997.
[5] Lauterborn W. Numerical Investigation of Nonlinear Oscillations of Gas-Bubbles in Liquids. JASA 1976; 59(2):283-293.
[6] Pierce A.D. Acoustics, An Introduction To Its Physical Principles And Applications, American Institute of Physics, 1994.
[7] Kinsler L.E, Frey A.F, Coppens A.B., Sanders J.V. Fundamentals of acoustics. John Wiley and Sons, INC, 2000.
[8] Akay A, Hodgson TH. Sound Radiation from An Accelerating Sphere. Journal of the Acoustical Society of America 1976; 59:S88.